

Microlensing by gas filaments

V. Bozza^{1,2,3*} and L. Mancini^{2,3†}

¹*Centro Studi e Ricerche “Enrico Fermi”, via Panisperna 89/A, Roma, Italy.*

²*Dipartimento di Fisica “E.R. Caianiello”, Università di Salerno, I-84081 Baronissi (SA), Italy.*

³*Istituto Nazionale di Fisica Nucleare, sez. Napoli, Italy.*

Received / Accepted

ABSTRACT

Gas in the interstellar matter is generally organized in filamentary structures, which may be also relevant for a complementary explanation of the dark matter in the Galactic halo. We examine the possibility that such structures may act as gravitational microlenses on background sources. To this purpose, we derive the general properties of a cylindrical lens and compare the light curves produced by such microlensing events with those generated by spherically symmetric clouds. We find that the establishment of the symmetry of the lens through the sole analysis of the light curve may be problematic, while the analysis of the astrometric shift of the centroid of the image can discriminate between the two classes of clouds. On the basis of our analysis, we find that only gas filaments with a very high density could be detectable. Such clouds are unlikely to exist in a long-lived state. Therefore, microlensing cannot discriminate on the existence and the relevance of gas filaments in the Halo, which could well be present and escape detection by ordinary microlensing surveys.

Key words: Gravitational lensing – ISM: clouds – ISM: structure

1 INTRODUCTION

In the last years, the idea that baryonic dark matter in the halo of our Galaxy could be in the form of self-gravitating cold gas clouds has roused a considerable debate. This gas may arise in the picture of a global fractal structure for the interstellar matter in the Galactic halo (Pfenniger, Combes & Martinet 1994; Pfenniger & Combes 1994; De Paolis et al. 1995a,b,c, 1996) (see also de Vega, Sanchez & Combes (1996) for a model of the “fractalization”). The presence of this gaseous component would help to account for the missing dark matter in the halo of the Galaxy avoiding problems with the initial mass function of compact objects helping to explain some observational puzzles. However, it is difficult to establish the existence and the relevance of such gas clouds on a clear observational ground.

In order to check this hypothesis, gravitational microlensing by gas clouds has been suggested by Henriksen & Widrow (1995). The lens masses requested to give detectable events are similar to those of the corresponding compact objects (MACHOs), i.e. of the order of a tenth of the solar mass, and the size should be of the order of the Einstein radius (few AU). They also suggest that these clouds could be responsible for the extreme scattering events

(ESE) (Fiedler et al. 1994), which affect the radio emission of Quasars. This hypothesis has been investigated and developed by Walker & Wardle (1998), who pointed out that the ESEs could be explained by a Galactic halo population of $\sim 10^{14}$ gas clouds, each of them having an ionized envelope. In this way, the ESE are generated by the motion across the line of sight of a lensing plasma which is able in principle to amplify and deamplify an extragalactic point radio source (see also Walker (1999); Walker, Wardle & Ohishi (2003)). De Paolis et al. (1999a) have drawn attention on the gamma ray emission of the gas clouds due to cosmic ray scattering. This gamma ray could be recognized in Dixon et al. (1998) detection according to De Paolis et al. (1999b). The details of the gamma ray production from cosmic ray scattering have been studied by Sciamia (2000).

Gerhard & Silk (1996) have discussed the observational consequence of the presence of cold gas clouds distributed in an extended, flattened, three-dimensional halo. These authors have also considered possible mechanisms to stabilize the gas clouds against gravitational collapse and star formation (see also Wardle & Walker (1999)). If the gas clouds were opaque, the microlensing surveys would detect the occultation of the source stars (Gerhard & Silk 1996; Walker & Wardle 1998). On the other hand, if the clouds were transparent at optical wavelengths, classical refraction could supply an alternative amplification mechanism (Draine 1998). Moreover, a gaseous lens would impose narrow infrared and far-red H_2 absorption lines on the back-

* E-mail: valboz@sa.infn.it

† lmancini@sa.infn.it

ground stellar spectrum. Existing programs to observe gravitational microlensing, supplemented by spectroscopy, can therefore be used to either detect such events or constrain the number of such gas clouds present in the Galaxy (Draine 1998). The magnification event rate has also been calculated for the case of gaseous lensing of stars in the Large Magellanic Cloud (LMC) by Rafikov & Draine (2001).

Bozza et al. (2002) studied an intermediate possibility: if gas clouds are effectively present in the halo, they could be likely associated to massive compact halo objects (MACHOs). If this is the case, these Pointlike Lenses Associated to Gas (PLAG) would be missed by standard microlensing observations, because their light curve would be significantly altered by the surrounding gas cloud. On the other hand, isolated gas clouds could be quite difficult to detect without a powerful amplification mechanism. In PLAGs, gravitational lensing by the central object would provide this mechanism, but secondary effects due to the cloud would show up in a weak or strong fashion, depending on the density of the diffuse matter. Significant differences in microlensing light curves of background sources are present also in the case of binary systems in a state of strong interaction, where mass exchanges, accretion disks, common envelopes provide circumstellar matter which can generate chromatic absorption effects (Bozza & Mancini 2002).

Kerins, Binney & Silk (2002) have examined the possibility that the data sets of microlensing experiments searching for MACHOs can also be used to search for occultation signatures by opaque gas clouds. Drake & Cook (2003) examining the MACHO project light curves of 48×10^6 stars towards the Galactic bulge, LMC and Small Magellanic Cloud (SMC), have found no presence of dark cloud extinction events. On an extragalactic ground, gas clouds could generate microlensing signature on distant quasars (Tadros, Warren & Hewett 1998). Up to now, no positive detection has been reported by microlensing surveys on quasars behind Virgo cluster.

So far, the relevance of gas clouds for gravitational microlensing has been discussed only in the case of spherically symmetric clouds (Henriksen & Widrow 1995). However, in general, the gas dynamics tends to form complex structures with lower symmetry, such as filaments and sheets. These structures are typically induced by external perturbations like shock waves from supernovae, which are the prime engine for fragmentation and star formation in molecular clouds (Larson 2003). The existence of a filamentary structure within interstellar gas clouds has been supported by numerical simulations and by many observations as well.

The theoretical studies of the structure of polytropic and isothermal cylinders have been carried out by Ostriker (1964, 1965). Stability analyses for the incompressible case have been performed by Chandrasekhar & Fermi (1953) and for the isothermal case by Stodolkiewicz (1963). The study of the fragmentation mechanism into filaments and then into stars has been investigated by Larson (1985) and later on by many authors. For a comprehensive review, see Larson (2003). The presence of magnetic fields and rotational motion play an important role in the definition of privileged directions for the formations of filaments, exerting always a slight stabilizing effect against gravitational collapse (Nakamura 1984; Nakamura et al. 1995). The dynamical evolution of clouds is also influenced by the global properties

of the internal turbulence (Klessen & Ballesteros-Paredes 2004). In any case, the most efficient factor preventing a cloud from collapsing is its internal temperature.

Filamentary structures appear to be present all around the Galaxy at all scales and in all dynamical components, ranging from molecular clouds with high rates of star formation (Schneider & Elmegreen 1979; Myers et al. 1991) to the regions surrounding the Galactic center (La Rosa et al. 2004), from intermediate and high velocity clouds in the Galactic halo (Richter et al. 2003) to molecular structures in the Magellanic Clouds (André et al. 2004). Even the various processes that rule the gas circulation through the Milky Way halo, such as the “Galactic Fountains” or matter debris torn from satellite galaxies caused by Milky Way tidal forces (the Magellanic stream is an example), rearrange the galactic gas preferably in filamentary shapes.

From this general discussion, we draw two considerations. Firstly, to investigate the observational effects of gaseous matter in the Galaxy, it is mandatory to discuss clouds with cylindrical symmetry, rather than spherical. Secondly, the actual limits of the microlensing technique as a tool for the investigation of diffuse interstellar matter still need to be established. At the present time, it is not clear whether microlensing surveys should expect events produced by gas clouds, and whether microlensing statistics can be used for an investigation of the relevance of diffuse components in the Galaxy. The absence of positive detections is not significant, since a serious analysis should start from a deep afterthought of the selection criteria.

To our knowledge, gravitational lensing by cylindrical lenses has not been considered before, except for a study by Bazin & De Freitas (1987). The aim of the present work is to perform an analytical investigation of this subject, with the purpose to establish the minimal requirements to the parameters of a gas filament in order to produce a detectable microlensing event. Besides this main target, we will also compare gravitational lensing by gas filaments with lensing by spherical clouds and cosmic strings.

The paper is structured as follows: in Sect. 2 we discuss the general properties of the cylindrical lens. In Sect. 3 we compare with the spherically symmetric case, showing that any microlensing light curve generated by a spherically symmetric distribution can be obtained by a cylindrical distribution, while the converse is not true. In Sect. 4 we show that the degeneracy can be fully broken using astrometric observations. In Sect. 5 we compare gas filaments with cosmic strings from the gravitational lensing point of view. Finally, in Sect. 6 we draw the conclusions, discussing the relevance of microlensing for the investigation of diffuse matter in the Galactic halo.

2 THE CYLINDRICAL LENS

As it is well known in the classical gravitational lensing theory, if the size of the lens is much smaller than its distance from the source and the observer, only the projected density distribution is relevant for gravitational lensing. We define the critical surface mass density as

$$\Sigma_{cr} = \frac{c^2 D_{OS}}{4\pi G D_{OL} D_{LS}} \quad (1)$$

and use a normalized surface density $\kappa(\mathbf{x}) = \Sigma(\mathbf{x})/\Sigma_{cr}$ (Schneider, Ehlers & Falco 1992). As usual, D_{OL} , D_{LS} and D_{OS} indicate the distance between observer and lens, lens and source, observer and source, respectively.

A cylindrical lens with infinite length is projected to a density distribution which is independent of one direction of symmetry. Taking this direction to be the x_2 axis of the lens plane, the generic density distribution takes the form

$$\kappa(x_1, x_2) = \lambda\sigma(x_1), \quad (2)$$

where $\sigma(x)$ is an even function normalized in such a way that

$$\int_{-\infty}^{+\infty} \sigma(x) dx = 1. \quad (3)$$

Then λ becomes the linear density of the filament, which is supposed to be constant, or negligibly variable on the scales relevant for microlensing.

The lens equation in the x_2 direction is trivial, since by symmetry no deviation is expected. Working in normalized coordinates (Schneider, Ehlers & Falco 1992), the deflection in the x_1 direction is

$$\begin{aligned} \alpha(x_1) &= \frac{1}{\pi} \int_{\mathbb{R}^2} \lambda\sigma(x'_1) \frac{x_1 - x'_1}{(x_1 - x'_1)^2 + (x_2 - x'_2)^2} dx'_1 dx'_2 = \\ &= 2 \int_0^{x_1} \lambda\sigma(x'_1) dx'_1. \end{aligned} \quad (4)$$

The lens equation is then simply

$$y_1 = x_1 - \alpha(x_1) \quad (5)$$

with its Jacobian being

$$J = \begin{pmatrix} 1 - 2\lambda\sigma & 0 \\ 0 & 1 \end{pmatrix}. \quad (6)$$

Critical curves occur whenever

$$\kappa = \lambda\sigma = 1/2. \quad (7)$$

They are described by the equation $|x_1| = x_c$, with $2\lambda\sigma(x_c) = 1$. By this equation, the critical curves are given by lines parallel to the filament on each side. The caustics corresponding to each critical line follow the equation $y_1 = y_c = \pm(x_c - \alpha_1(x_c))$, which still describes two lines parallel to the filament but in the source plane.

Thanks to the high symmetry of this class of lens models, the general theory has taken very few steps. It is however instructive to visualize the main properties of the cylindrical models on a specific example. To this purpose, we shall take for $\sigma(x_1)$ a gaussian profile with width σ_0

$$\sigma(x_1) = \frac{1}{\sigma_0\sqrt{2\pi}} e^{-x_1^2/2\sigma_0^2}. \quad (8)$$

The deflection angle of such a density distribution is

$$\alpha(x_1) = \lambda \operatorname{Erf} \left(\frac{x_1}{\sigma_0\sqrt{2}} \right). \quad (9)$$

Strictly speaking, this formula is valid for $|x_1| \ll l$, where l is the length of the filament. In the opposite limit, when $|x_1| \gtrsim l$ the integration on x_2 in Eq. (4) should be performed carefully, so that at very large x_1 we recover the

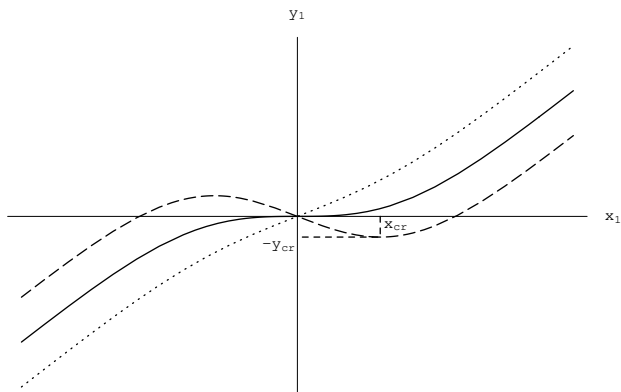


Figure 1. The lens equation for a cylindrical lens with a gaussian density profile for different values of the linear density. The solid line has $\lambda = \lambda_{cr}$, the dotted line $\lambda = 0.5\lambda_{cr}$ and the dashed line $\lambda = 1.5\lambda_{cr}$.

Schwarzschild lens behaviour. However, in the context of this paper, we stick to the case $x_1 \ll l$, where we expect the cylindrical lens effects to become important. In this limit, the deflection angle is correctly represented by Eq. (4).

In the particular case of a gaussian density profile, in Fig. 1 we plot the lens equation obtained using Eq. (9) for different values of the linear density λ . As the gaussian has its maximum at $x_1 = 0$, we can define a critical linear density

$$\lambda_{cr} = \sigma_0 \sqrt{\frac{\pi}{2}}, \quad (10)$$

such that for $\lambda < \lambda_{cr}$ the Jacobian is always positive and we have no critical curve, while for $\lambda > \lambda_{cr}$ we have two critical curves. Since for a cylindrical lens the Jacobian reduces to the derivative of the lens equation, we can directly identify the critical curves with the local extrema of the lens equation. For example, in Fig. 1, the $\lambda = 0.5\lambda_{cr}$ curve is monotonic, the $\lambda = \lambda_{cr}$ curve has a degenerate stationary point in $x_1 = 0$ and the curve for $\lambda = 1.5\lambda_{cr}$ has two symmetric extrema at $x = \pm x_{cr}$, which correspond to two critical curves on each side of the filament. The height of the extrema determines the position of the corresponding caustics y_{cr} . So, if y is in the range $|y| < y_{cr}$, we have three solutions for the lens equation, two with positive parity at positions $|x| > x_{cr}$ and one in the middle with negative parity. The parity can be directly read as the sign of the derivative of the lens equation.

At this point we can draw some microlensing light curve samples based on this filament model. What counts in a microlensing event is the projected relative velocity between source and lens. As usual, we set ourselves in the frame where the lens is fixed in the sky and the source moves with respect to it. In our hypothesis of uniform filament, we have an additional symmetry along the y_2 axis, so that only the velocity component v_1 along y_1 is relevant. In practice, any microlensing event starts with a source at $y_1 = -\infty$, then develops with a source passing through $y_1 = 0$ and will end up with the source at $y_1 = +\infty$.

In order to draw a microlensing light curve, we have to solve the lens equation (5) with $y_1 = v_1 t$ and sum the magnifications of all images, given by the absolute value of the

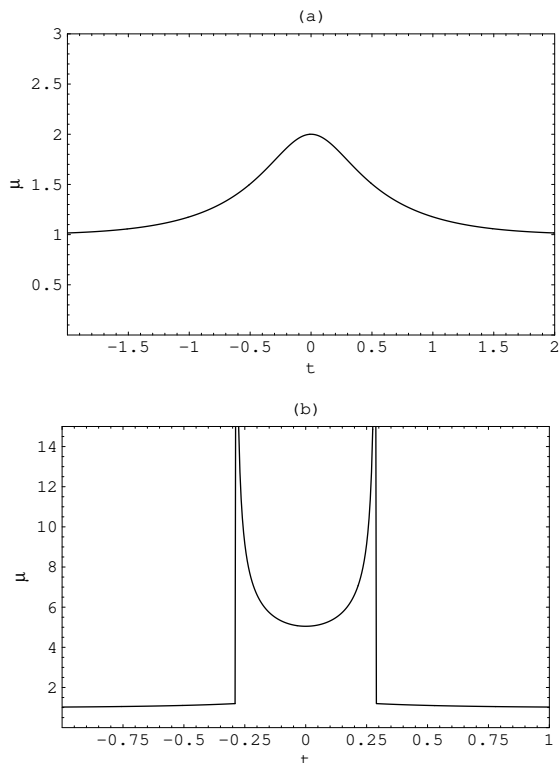


Figure 2. Microlensing light curves for a cylindrical lens with a gaussian density profile with $\sigma_0 = 1$: (a) $\lambda = 0.5\lambda_{cr}$, (b) $\lambda = 1.5\lambda_{cr}$. Time is normalized in such a way that $t = 1$ corresponds to $y_1 = 1$.

inverse of the Jacobian determinant evaluated at the image positions. We can distinguish two cases: an underdense filament $\lambda < \lambda_{cr}$ and an overdense filament $\lambda > \lambda_{cr}$. In the first case (Fig. 2a) we always have one image and the light curve is single-peaked resembling the Paczynski curve or the light curves drawn by Henriksen & Widrow (1995). In the second case (Fig. 2b) we always have a caustic crossing event, as the caustic runs along the whole filament. The light curve then is characterized by two symmetric spikes and a central flat region, resembling the light curves of binary lenses or those produced by diffuse clouds with extended caustics.

3 COMPARISON BETWEEN THE LIGHT CURVES GENERATED BY CYLINDRICAL AND SPHERICAL LENSES

Looking at the light curves shown in Fig. 2 a very important question arises: is it possible to identify the symmetry of the lens (cylindrical or spherical) from any peculiarities of the light curves? This question is not at all of academic interest, but becomes of primary importance as soon as we want to study the properties of the lensing object from the microlensing light curves that we observe. The shape and the extension of the clouds, together with their density are needed to estimate the total mass of the object and, on a large statistic, the relevance of the cloud population for the total matter in the halo.

In this section we will prove a simple theorem stating that any light curve produced by a spherically symmetric lens can be reproduced by a cylindrical lens with a suitable density profile. The converse turns out to be not true. In fact, only a specific class of cylindrical density profiles can be mimicked by spherically symmetric ones.

Consider a spherical lens, with density profile $\sigma_s(x_s)$, which is a function of the radial coordinate x_s in the lens plane. The spherical lens equation reads

$$y_s = x_s - \frac{m(x_s)}{x_s}, \quad (11)$$

where

$$m(x_s) = 2 \int_0^{x_s} x' \sigma_s(x') dx' \quad (12)$$

is the dimensionless mass enclosed in the radius x_s (Schneider, Ehlers & Falco 1992).

The magnification of each image is given by

$$\mu_s(x_s) = \frac{1}{\frac{y_s(x_s)}{x_s} y'_s(x_s)}. \quad (13)$$

Here we consider the case of a microlensing event with no caustic crossing, hence with a single positive parity image. We refer the reader to the appendix for the more complicated case of a caustic crossing event.

We start by writing the source position as a function of time

$$y_s = \sqrt{b^2 + v_s^2 t^2}, \quad (14)$$

where v_s is the relative velocity between source and lens and b is the impact parameter of the source trajectory with the optical axis (the line connecting observer and lens).

The light curve is found inverting the lens equation (11) for each y_s and evaluating the magnification on the image position using (13).

On the other hand, the cylindrical lens is characterized by a density distribution $\lambda\sigma_c(x_c)$, which is a function of the coordinate x_c transverse to the filament axis in the lens plane. Its lens equation is

$$y_c = x_c - 2\lambda \int_0^{x_c} \sigma_c(x') dx' \quad (15)$$

and the magnification is

$$\mu_c(x_c) = \frac{1}{\frac{dy_c}{dx_c}} = \frac{1}{1 - 2\lambda\sigma_c(x_c)}. \quad (16)$$

In a microlensing event, as said before, the source position is $y_c = v_c t$, where v_c is the component of the source velocity transverse to the filament axis.

Our aim is to show that for any microlensing event caused by a spherically symmetric lens characterized by σ_s , b , v_s there exist a microlensing event caused by a filament with some σ_c and v_c such that the two light curves coincide.

The theorem can be stated by the equality between the magnifications as functions of time

$$\mu_s(x_s(y_s(t))) = \mu_c(x_c(y_c(t))). \quad (17)$$

In both cases we have written the source position as

function of time. Eliminating t , we get a relation between the source positions in the two microlensing events

$$y_s^2 = b^2 + r_v^2 y_c^2 \quad (18)$$

where $r_v = v_s/v_c$.

Solving with respect to y_c and deriving with respect to x_c we get

$$\frac{y_s}{r_v \sqrt{y_s^2 - b^2}} \frac{dy_s}{dx_s} \frac{dx_s}{dx_c} = \pm \frac{dy_c}{dx_c}. \quad (19)$$

On the r.h.s. we have $1/\mu_c = 1/\mu_s$. Substituting Eq. (13) we finally get

$$\frac{dx_s}{dx_c} = \pm \frac{r_v}{x_s} \sqrt{y_s^2(x_s) - b^2}, \quad (20)$$

where the plus sign holds for positive parity images and the minus sign holds for negative parity ones. In a non-caustic crossing event, only a positive parity image is present. We shall thus take the plus sign.

This is a differential equation which gives us x_s as a function of x_c , relating the positions of the images in the two microlensing events. If there were no lens, Eq. (20) would be solved by $x_s = \sqrt{b^2 + r_v^2 x_c^2}$. The presence of the lens modifies this relation at low x_c , since when the source has minimum impact parameter, its image is no longer just $x_s = b$ but we have to solve the lens equation, finding $x_s(0) = y_s^{-1}(b)$. This dictates the initial condition we need to solve the differential equation (20). The r.h.s. can be explicitly expressed in terms of x_s using the spherical lens equation, so that for any density profile σ_s , any impact parameter b and velocity ratio r_v we can get a family of curves $x_s(x_c)$. These can be used to construct a filament density profile using Eqs. (16) and (17)

$$\lambda \sigma_c(x_c) = \frac{1}{2} \left(1 - \frac{1}{\mu_s(x_s(x_c))} \right). \quad (21)$$

In Fig. 3 we show the results of this procedure starting from a spherically symmetric lens with a gaussian density profile (Fig. 3b). The equation which relates x_s to x_c has been solved numerically and shown in Fig. 3a for different impact parameters. Finally, the corresponding density profiles for the filament are shown in Fig. 3c. Of course, to a given spherically symmetric density profile we cannot associate a unique equivalent cylindrical profile, but rather a family of profiles which depend on the impact parameter of the microlensing event we want to reproduce and the velocity ratio of the two microlensing events. While the latter is only a scale factor between x_c and x_s , the impact parameter determines the central density of the filament. The lower the impact parameter, the higher the central density. For $b = 0$, we get the relation

$$\sigma_c(0) = \frac{1}{2\pi} [1 - (1 - \sigma_s(0))^2], \quad (22)$$

which also tells us that for any subcritical spherically symmetric density

$$\sigma_c(0) < \frac{\sigma_s(0)}{\pi}. \quad (23)$$

So, looking at Fig. 3c we deduce that any microlensing event generated by a spherically symmetric distribution can be explained by some filamentary distributions. However, the latter need generically a lower central density to generate

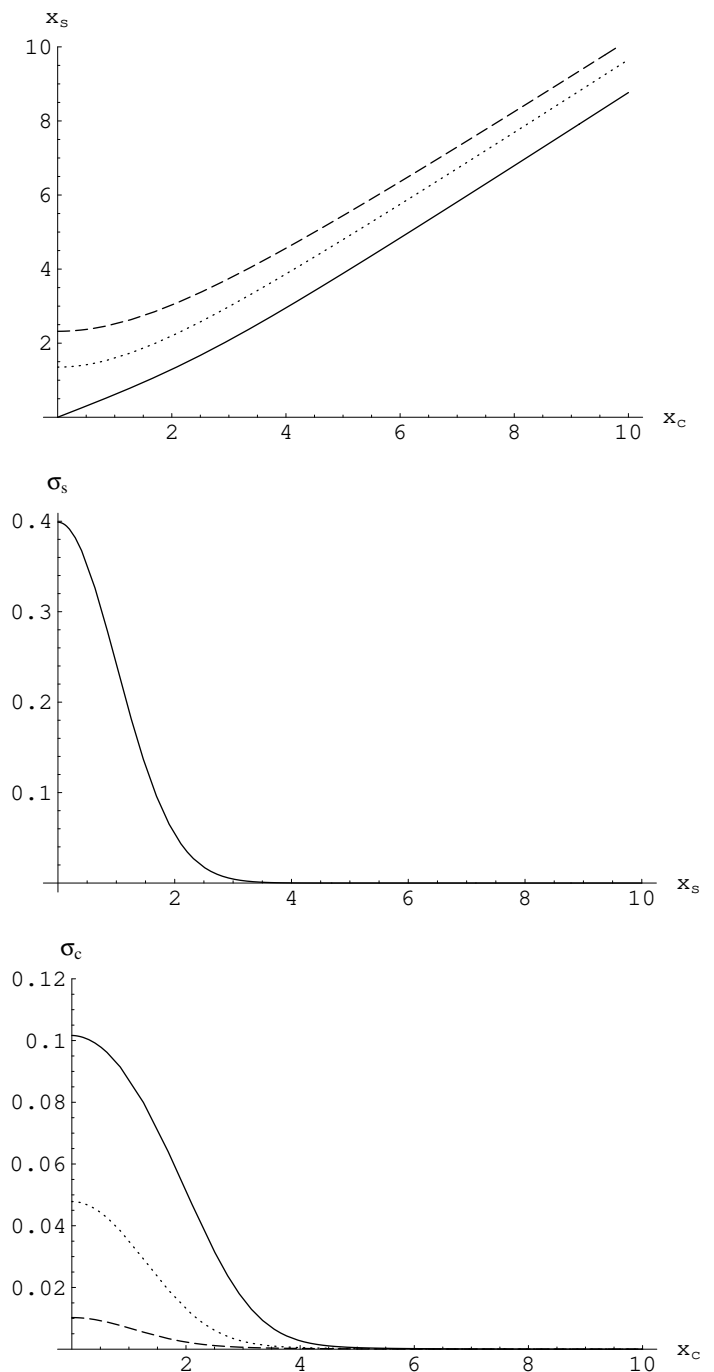


Figure 3. Given a spherically symmetric gaussian density distribution shown in (b), (a) shows the relation between the spherical lens image position x_s and the corresponding cylindrical lens image position x_c . (c) shows some cylindrical density profiles which reproduce the same microlensing event as (b) for different impact parameters: the solid line is for $b = 0$, the dotted for $b = 1$ and the dashed for $b = 2$.

the same peak magnification. The required central density is suppressed even more as soon as b departs from zero (see discussion in Sect. 6).

A general property of spherically symmetric lenses is that the tail of the event must follow a universal law

$$\mu_s \simeq 1 + c_1 t^{-4}. \quad (24)$$

This can be seen as follow. The Jacobian determinant of the spherical lens is

$$\det J_s = \left(1 - \frac{m(x_s)}{x_s^2}\right) \left(1 + \frac{m(x_s)}{x_s^2} - 2\sigma_s(x_s)\right). \quad (25)$$

Since the total mass of the distribution should be finite, $m(x_s)$ should converge to a finite value $m(\infty)$. In order for this to occur, σ_s should drop faster than x_s^{-2} . As a consequence, the dominant terms are

$$\det J_s \simeq 1 - \frac{m^2(\infty)}{x_s^4}. \quad (26)$$

At the tail of the event we have $x_s \simeq y_s \simeq v_s t$, and then the magnification goes as

$$\mu_s \simeq 1 + \frac{m^2(\infty)}{v_s^4 t^4}. \quad (27)$$

For the cylindrical lens we have no similar universal behaviour. The tail of the event follows the tail of the distribution. From Eq. (16), for large t we find

$$\mu_c \simeq 1 + 2\lambda\sigma(v_c t). \quad (28)$$

This suggests that only a special class of cylindrical microlensing events can have the correct form to be compatible with a spherically symmetric explanation, namely the density profiles falling as x_c^{-4} at large distances from the filament axis. For example, the light curves shown in Fig. 2 cannot be obtained by a spherically symmetric lens. However, this general statement can be applied to physical events only within the uncertainties, since a true spherically symmetric event may have a first long tail coming from its diffuse distribution which hides the last t^{-4} tail behind the noise.

In the case of caustic crossing microlensing events, the search for an equivalent cylindrical lens is complicated by the creation/destruction of pairs of images. However, it can be indeed proved that the theorem continues to hold. In the appendix, we give an algorithm to generate a cylindrical density profile from a caustic crossing microlensing event induced by a spherical cloud which reproduces the same light curve.

4 ASTROMETRIC MICROLENSING BY GAS CLOUDS

Astrometric measurements on the position of the centroid of the star suffering microlensing were first proposed by Walker (1995) and Høg, Novikov & Polnarev (1995) (see also Dominik & Sahu (2000)). They are based on the fact that even if we cannot resolve all the images individually, if we have enough resolution (of the order of the Einstein radius in the case of a pointlike lens), we can at least detect a shift in the centroid of the lensed star, which follows the movement of the images. In the case of a pointlike lens, it

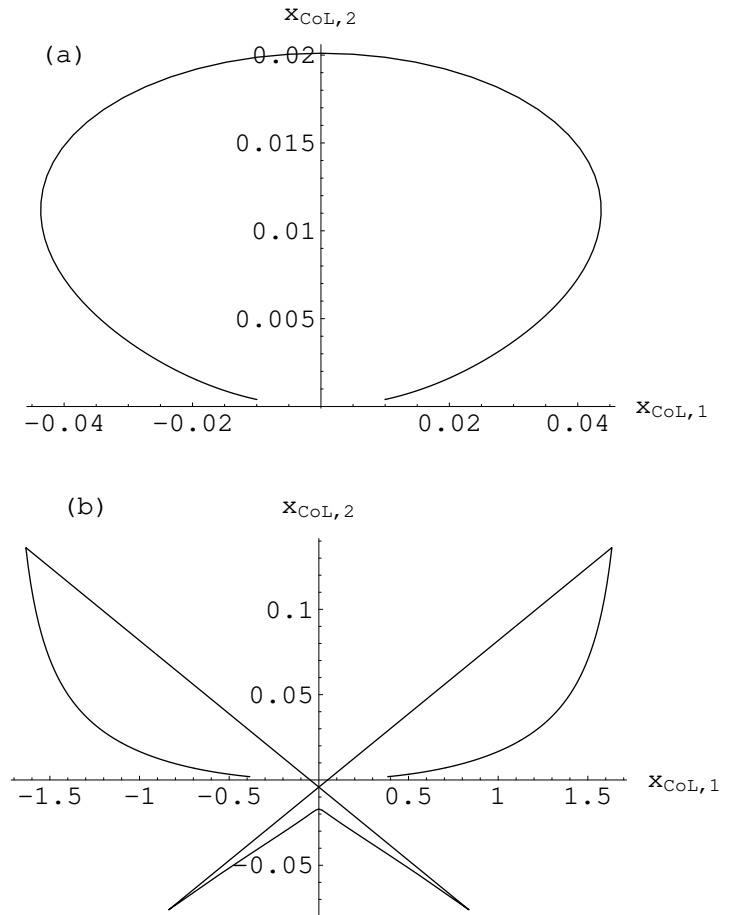


Figure 4. Center of light trajectories for a spherical cloud with gaussian density. (a) A non-caustic crossing event. (b) A caustic crossing event.

is well known that the center of light (CoL) describes an ellipse in the sky, which can be used for a better estimate of the microlensing parameters.

Now let us consider a gas cloud as a lens with a spherical density profile. The procedure to follow to calculate the CoL trajectory is straightforward. We have to solve the lens equation for $y = \sqrt{b^2 + v_s^2 t^2}$, calculate the magnification $\mu^{(i)}$ of each image $x^{(i)}$ and evaluate a weighed average

$$x_{\text{CoL}} = \sum \frac{x^{(i)} \mu^{(i)}}{\mu_{\text{tot}}} - y, \quad (29)$$

where we have to subtract the position of the source in order to get into the correct frame (the frame where the source is steady and the lens moves). Up to now, the CoL curves for a diffuse spherical lens have not been shown. In Fig. 4 we show two examples obtained with a gaussian density profile. In Fig. 4a we show the CoL trajectory in a microlensing event where the source does not cross any caustics. In this case, we always have only one image and the CoL position is just the difference between the image and the source position. The trajectory is no longer an ellipse, but develops an asymmetry between $t = 0$ (the upper part of the curve) and $t = \pm\infty$ (the lower part). This asymmetry depends on the density profile

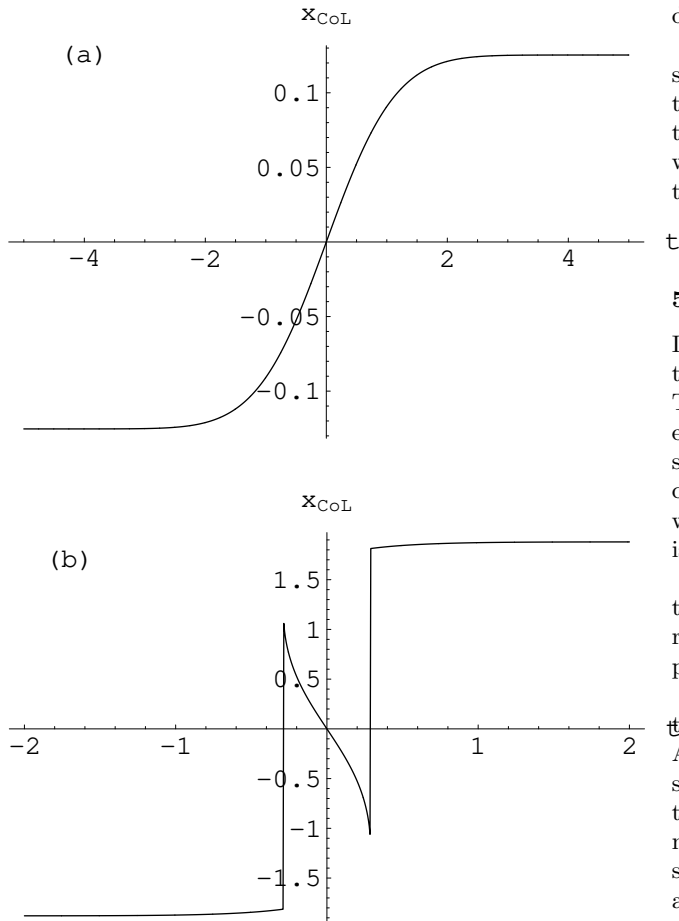


Figure 5. Center of light trajectories for a filament with gaussian transverse density. (a) A non-caustic crossing event. (b) A caustic crossing event.

and can show up with an ellipse which is either flatter on the top (like the one shown here) or flatter on the bottom.

In Fig. 4b we show a case with a source which enters a radial caustic. Two more images are generated on the side opposite to the source, so that in the neighbourhood of $t = 0$, the CoL jumps in the lower half-plane (see Gould & Han (2000) for similar plots in binary microlensing).

Now let us consider a gas filament with a uniform linear density and a gaussian transverse density profile. The big difference with respect to the spherical lens is that now the CoL motion takes place only along one direction, namely the direction transverse to the filament. In Fig. 5a we show the motion of the CoL as a function of time. Notice that, since we are considering an infinite filament, the CoL does not return to zero at large times. Actually, for a finite size filament this would obviously occur, but at times very far from the luminosity peak. By the cylindrical lens equation (5), we see that the starting position for the CoL is $-\lambda$ and the final position is $+\lambda$. So an observer looking at the star during the microlensing event, would measure a shift equal to 2λ in the direction transverse to the filament. This CoL motion is absolutely different from the CoL motion of the spherical case.

Therefore the CoL motion provides a very clear criterion to discriminate between the two kinds of symmetries.

In Fig. 5b we have a caustic crossing event. Like in the spherically symmetric case, two more images are present in the neighbourhood of $t = 0$, which make the CoL jump on the opposite side. The curve passes through 0 at $t = 0$, where we have two symmetric images on opposite sides of the filament and a third image at the center.

5 GAS FILAMENTS VS. COSMIC STRINGS

In the recent years, particular attention has been devoted to the study of cosmic strings (Zeldovich 1980; Vilenkin 1981). These are topological defects which may develop after high energy cosmological phase transitions. To visualize a cosmic string, one may firstly consider a circle on the plane. If we cut a sector from the circle and glue the two cuts together, we obtain a conical surface. In a similar way, a cosmic string is the cusp of a conical three-dimensional space.

Since gaseous filaments have the same spatial symmetries as cosmic strings, one may ask whether there are any relations or similarities between the gravitational lensing properties of the two classes of objects.

Following Gott (1985), a cosmic string does not change the curvature of the target spacetime, but only the topology. As a consequence, light rays are not deflected by a cosmic string. However, because of the conical structure of spacetime, two light rays passing on different sides of the string may converge later at the same arrival point. If a cosmic string lies between us and a distant source, we see two images of the source separated by an angle

$$\Delta\theta = 8\pi\mu_s \sin\alpha \frac{D_{LS}}{D_{OS}}, \quad (30)$$

where μ_s is the string linear density and α is the angle between the string and the direction from the observer to the source. The two images are identical to the original source, with no amplification or distortion. This is to be contrasted with the gravitational lensing by gas filaments, where we have one or three elongated images.

If we are in a typical microlensing situation, with a string passing in front of the source and the two images unresolved, then we can distinguish two cases, depending on the ratio between $\Delta\theta$ and the source diameter. In fact, if this ratio is larger than one, then the apparent luminosity of the source would be rapidly doubled, as the second image appears. Then it would stay constant for some time and finally return to the original value, as the first image disappears.

If $\Delta\theta$ is smaller than the source size, then only a portion of the source is doubled. The total amplification stays smaller than two and we have a peculiar single peak curve, without long tails, with a shape depending on the luminosity profile of the source.

Summing up, we see that gravitational lensing by cosmic strings is structurally different from classical gravitational lensing by ordinary matter. It would be very difficult to bump into ambiguous cases. For their peculiar properties, cosmic strings have been invoked several times to explain twin objects showing no apparent distortion (Turner, Schneider, Burke et al. 1986; Sazhin et al. 2003).

6 DISCUSSION AND CONCLUSIONS

Gas clouds have been invoked as a possible alternative explanation for halo dark matter using ordinary baryonic constituents. Their presence would represent a more orthodox solution to the problem with respect to exotic particles and would solve some observational puzzles. However, it is difficult to clearly prove this hypothesis and to quantify its relevance in the dark matter problem.

In this work we have revisited the original idea of microlensing by spherical gas clouds by Henriksen & Widrow (1995), extending to the case of gaseous filaments, which is the most likely geometry assumed in a realistic picture. If we restrict ourselves to a light curve analysis, then we proved in Sect. 3 that any microlensing event generated by a spherically symmetric distribution can be explained by a filamentary distribution, while the converse is not true. The degeneracy between the two classes of events can be broken by astrometric observations of CoL motion, since this would be one-dimensional for cylindrical lenses and two-dimensional for spherical ones.

A very important fact about filamentary clouds is that the study of a microlensing event generated by them can be used for a precise reconstruction of the density profile through Eqs. (15) and (16). This because any microlensing event would probe the whole transverse structure of the filament, including the center. In spherical clouds, instead, the presence of an additional parameter (the impact parameter) does not allow a univocal reconstruction of the density profile.

It is also important to remark that filaments are generally more efficient microlenses than spherical clouds since, given a central density of the cloud, a filament would give a higher magnification for microlensing. In fact, the best magnification that can be obtained by a spherical cloud is for a zero impact parameter event. In this case, Eq. (23) shows that spherically symmetric clouds require a slightly larger central density than cylindrical ones in order to give the same magnification. Of course, for larger impact parameters the difference would increase even more.

Similarly to what happens for spherical clouds (Henriksen & Widrow 1995; Draine 1998; Bozza et al. 2002), cold gas causes reddening of the light of the background source due to absorption by Rayleigh scattering. As a consequence, a high chromaticity in the light curve could be expected. Spectroscopic measurements during these microlensing events would yield a precise knowledge of the chemical composition of the clouds. Of course, such detailed analysis could be performed in a completely renewed framework for microlensing surveys, with selection criteria completely redesigned to unveil microlensing events generated by gas clouds.

As regards the microlensing probability in a given model of gas distribution, we need to specify three parameters: the total mass in gas clouds, the central density ρ_0 and the typical transverse size σ_0 of a single cloud. This is to be contrasted with the MACHO picture, where the last two parameters are replaced by a single one, namely the mass of the MACHO. Of course, in any realistic model of the baryonic halo, we should replace the mass of the MACHO with a mass function. In the same way, for an ensemble of gas clouds, we would have a distribution $dN/d\rho_0 d\sigma_0$, rather

than a single value for ρ_0 and σ_0 . An important fact is that one can easily find that the total microlensing probability is independent of the shape of the cloud. So, for example, the frequency of microlensing events generated by a population of filamentary clouds would be exactly the same as for a population of spherical clouds with the same total mass and similar transverse size. This allows us to neglect higher order shape parameters to determine the microlensing probability.

Now let us analyze the minimal requirements for the parameters of a gas filament in order to be detectable by present microlensing surveys. A typical microlensing campaign puts a threshold on the minimal amplification and has a detection efficiency limited to events with duration within a specified range. For a typical event with maximum amplification at the peak $\mu_{max} = 2$, we shall now derive a relation between the duration and the central density. For our Gaussian density profile, we can easily write down the following relation between the central volume density ρ_0 , the linear density λ and the radius of the filament σ_0

$$\rho_0 = \frac{\lambda}{2\pi\sigma_0^2}. \quad (31)$$

By Eq. (16), we can immediately deduce the radius of the filament as a function of the central density and magnification at the peak

$$\sigma_0 = \frac{1}{2\rho_0\sqrt{2\pi}} \left(1 - \frac{1}{\mu_{max}}\right). \quad (32)$$

The semi-duration of the event can be quantified by $t_{1/2}$, which is the time needed to halve the amplification. It is defined by the relation

$$\mu(x_1(t_{1/2})) = \frac{\mu_{max} + 1}{2}. \quad (33)$$

By the lens equation (5),

$$t_{1/2} = \frac{1}{v} [x_{1/2} - \alpha(x_{1/2})], \quad (34)$$

where v is the relative projected velocity between source and filament and $x_{1/2}$ is defined by

$$\mu(x_{1/2}) = \frac{\mu_{max} + 1}{2}. \quad (35)$$

Then, by simple algebra, using (9) and restoring dimensional units we obtain

$$t_{1/2} = \frac{k_0 \Sigma_{cr}}{v \rho_0} \quad (36)$$

$$k_0 = \frac{\mu_{max} - 1}{4\sqrt{\pi}\mu_{max}^2} \left[\sqrt{\pi}(\mu_{max} - 1) \text{Erf} \left(\sqrt{\ln \frac{\mu_{max} + 1}{\mu_{max}}} \right) - 2\mu_{max} \sqrt{\ln \frac{\mu_{max} + 1}{\mu_{max}}} \right] = 0.05. \quad (37)$$

Fixing the maximum semi-duration to 150 days, the projected velocity to 200 km/s, and the chemical composition of the filament to H_2 molecules, we can calculate the central volume density of the filament for different observational targets (the geometry enters through the critical density Σ_{cr}). For example, if the source is a star in the LMC ($D_{OS} = 50$ kpc), the number density at the center of the filament should be at least $n_0 = 1.2 \times 10^{12} \text{ cm}^{-3}$. If the source is in M31 ($D_{OS} = 700$ kpc), we have $n_0 = 8.7 \times 10^{10} \text{ cm}^{-3}$. If the source is a quasar at 1 Gpc distance, we have

$n_0 = 6 \times 10^7 \text{ cm}^{-3}$. Of course, leaving fixed the magnification at the peak, which is a function of the product $\rho_0 \sigma_0$, we can lower the central density increasing the radius of the filament. However, the duration of the event is proportional to the inverse of ρ_0 and would rapidly become too long for a reasonable microlensing campaign. We can repeat the calculation changing the maximum amplification μ_{max} , but this only changes the final result by a numerical factor of order unity.

According to Henriksen & Widrow (1995) the typical molecular number density for spherical clouds required to generate appreciable gravitational lensing effects is even higher (10^{15} cm^{-3}) than what we have found. The higher densities experimentally measured for dark clouds are of the order of 10^5 cm^{-3} (Carroll & Ostlie 1996), while in massive star forming cloud, they may exceed 10^7 cm^{-3} in some locations (Evans 1999; Garay & Lizano 1999). Only quasar microlensing seems to have enough sensitivity to probe diffuse interstellar matter on the basis of present knowledge. This potentially interesting topic would thus deserve a separate study beyond the scope of this work.

As regards stellar microlensing on Galactic or Local-Group scales, the situation is not really promising. In fact, it is difficult to imagine a mechanism which keeps in a metastable state a gas cloud with density of the order of 10^{10} cm^{-3} for a sufficiently long life. Such density can only be reached during a collapsing stage for a relatively short time, even if global properties like magnetic field and internal turbulence partially contrast the gravitational collapse of the gas (Klessen & Ballesteros-Paredes 2004).

We conclude that only quasar microlensing can hope to say something on the presence and the relevance of diffuse clouds or filaments in the haloes of other galaxies. Galactic microlensing campaigns cannot give any definite answer to the question on the existence of a relevant diffuse baryonic component in the Galactic halo, unless completely new ideas intervene in the observational strategies or high density gas clouds are effectively sustained by some still unknown mechanisms. A positive detection of a microlensing event due to a purely diffuse cloud or filament would be a quite unrealistic chance, which could not help us to understand the global problem all the same, since it would be generated by a very peculiar object. On the other hand, the absence of signs of diffuse matter in present microlensing campaigns does not exclude the possibility of large distributions of filaments in the Halo, which would be too diluted to give appreciable microlensing effects. One possibility still remaining open is for gas clouds associated to compact objects (Bozza et al. 2002), which would provide an efficient microlensing amplification mechanism and signal the presence of gas in the Halo. Otherwise, the problem should definitely be tackled by other techniques.

ACKNOWLEDGMENTS

We thank the CERN theory department and the Institute for theoretical physics of the Zürich University for hospitality. We also thank Gaetano Scarpetta for careful reading of the manuscript.

REFERENCES

- Alcock C. et al., 2000, ApJ, 542, 281
 André M. K. et al., 2004, astro-ph/0404063
 Bazin M. J., De Freitas L., 1987, Ap&SS, 138, 381
 Bozza V., Jetzer Ph., Mancini L., Scarpetta, G., 2002, A&A, 382, 6
 Bozza V., & Mancini L., 2002, A&A, 394, L47
 Carroll B.W., Ostlie D.A., 1996, "An introduction to modern astrophysics" (Addison-Wesley Pub. Comp.)
 Chandrasekhar S., Fermi E., 1953, ApJ, 118, 116
 De Paolis F., Ingrassio G., Jetzer Ph., Roncadelli M., 1995, PRL, 74, 14
 De Paolis F., Ingrassio G., Jetzer Ph., Roncadelli M., 1995, A&A, 295, 567
 De Paolis F., Ingrassio G., Jetzer Ph., Qadir A., Roncadelli M., 1995, A&A, 295, 647
 De Paolis F., Ingrassio G., Jetzer Ph., Roncadelli M., 1996, Ap&SS, 235, 329
 De Paolis F., Ingrassio G., Jetzer Ph., Roncadelli M., 1999, ApJ, 510, L103
 De Paolis F., Ingrassio G., Jetzer Ph., Roncadelli M., 1999, astro-ph/9906083
 de Vega H. J., Sánchez N., Combes F., 1996, PRD, 54, 106008
 Dixon D. D. et al., 1998, Nat, 3, 539
 Dominik M., Sahu K., 2000, ApJ, 534, 213
 Draine B. T., 1998, ApJ, 509, L41
 Drake A. J., Cook K. H., 2003, ApJ, 589, 281
 Evans N. J., 1999, Ann. Rev. Astron. Astroph., 37, 311
 Fiedler R., Dennison B., Johnston K. J. et al., 1994, ApJ, 430, 581
 Garay G., Lizano S., 1999, Astron. Soc. Pacific, 111, 1049
 Gerhard O., Silk J., 1996, ApJ, 472, 34
 Gott J. R., 1985, ApJ, 288, 422
 Gould A., Han C., 2000, ApJ, 538, 653
 Henriksen R. N., Widrow L. M., 1995, ApJ, 441, 70
 Høg E., Novikov I. D., Polnarev A. G., 1995, A&A, 294, 287
 Kerins E., Binney J., Silk J., 2002, MNRAS, 332, L29
 Klessen R. S., Ballesteros-Paredes J., 2004, astro-ph/0402038
 Lasserre T., Afonso C., Albert J.N. et al., 2000, A&A, 355, L39
 La Rosa T. N., Nord M. E., Lazio T. J., Kassim N. E., 2004, astro-ph/0402061
 Larson R. B., 1985, MNRAS, 214, 379
 Larson R. B., 2003, Rep. Prog. Phys., 66, 1651
 Myers P. C., Fuller G. A., Goodman A. A., Benson P. J., 1991, ApJ, 376, 561
 Nakamura T., 1984, Prog. Theor. Phys., 70, 212
 Nakamura T., Hanawa T., Nakano T., 1995, ApJ, 444, 770
 Ostriker J., 1964, ApJ, 140, 1056
 Ostriker J., 1965, ApJ Suppl., 11, 167
 Pfenniger D., Combes F., 1994, A&A, 285, 94
 Pfenniger D., Combes F., Martinet L., 1994, A&A, 285, 79
 Rafikov R. R., Draine B. T., 2001, ApJ, 547, 207
 Richter P., Sembach K. R., Howk J. C., 2003, A&A, 405, 1013
 Sazhin M., Longo G., Capaccioli M. et al., 2003, MNRAS, 343, 353
 Schneider S. S., Elmegreen B. G., 1979, ApJ, 41, 87

- Schneider P., Ehlers J., Falco E. E., 1992, *Gravitational Lenses* (Springer Verlag)
- Sciama D. W., 2000, MNRAS, 312, 33
- Stodolkiewicz J. S., 1963, Acta Astronomica, 13, 30
- Tadros H., Warren S., Hewett P., 1998, New Astronomy Reviews, 42, 115
- Turner E. L., Schneider D. P., Burke B. F. et al., 1986, Nature, 321, 142
- Vilenkin A., 1981, PRD, 23, 852
- Walker M. A., 1995, ApJ, 453, 37
- Walker M., 1999, MNRAS, 306, 504
- Walker M., Wardle M., 1998, ApJ, 498, L125
- Wardle M., Walker M., 1999, ApJ, 527, L109
- Walker M., Wardle M., Ohishi M., 2003, ApJ, 589, 810
- Zeldovich Ya. B., 1980, MNRAS, 192, 663

APPENDIX A: COMPARISON BETWEEN THE LIGHT CURVES GENERATED BY CYLINDRICAL AND SPHERICAL LENSES: CAUSTIC CROSSING EVENTS

In this appendix we extend the theorem of Sect. 3 to caustic crossing microlensing events. Suppose we have a spherically symmetric distribution which exceeds the critical surface density in a neighbourhood of its center. Then we shall have a tangential critical curve when $m(x_s) = x_s^2$ and an inner radial critical curve when $dy_s/dx_s = 0$. The caustic corresponding to the tangential critical curve is just a point on the optical axis, while the caustic corresponding to the radial critical curve is a circle of finite size, which can be crossed by a source with a sufficiently small impact parameter. Here we shall consider the case of a single radial critical curve.

In the spherically symmetric case, we have a principal image which is not involved in creation/destruction processes. Then, when the source enters the caustic, an additional pair of image forms: one in the range between the tangential critical curve and the radial critical curve and another between the radial critical curve and the origin.

In the cylindrical case, we have one image on the same side of the source when this is outside the caustic. Then, when the source enters the caustic, two images are generated on the opposite side: one moves away from the filament and the other moves towards the center of the filament, both starting from the critical line. When the source is aligned with the filament, we have a symmetric situation where the original image and the second one are outside the critical lines on specular positions and the third one is right at the center.

When we have more than one image, in principle we can distribute the total magnification among the images in arbitrary proportions. For each choice we can find a different cylindrical density profile. Just to prove the existence of at least one profile, we impose that to any image in the spherically symmetric case, there corresponds one image in the cylindrical case which has the same magnification. Our choice is to identify the most external images each other and to identify the two remaining ones by their parity. Even with this simple choice, the procedure to find $x_s(x_c)$ is somewhat complicated.

Eq. (20) can still be used to relate the positions of the

images, though we should take care of the sign of the images. To obtain the three images, we have to start by suitable initial conditions. In fact, when the source reaches its minimum distance b from the center, the spherical lens equation yields three solutions that we can label in decreasing order as $x_s^{(i)}$ with $i = 1, 2, 3$. For the negative parity images the logical choice is $x_s(0) = x_s^{(2)}$. The differential equation (20) with the minus sign can then be followed without singularities even through the radial critical curve until y_s becomes equal to b . This happens when x_s reaches $x_s^{(3)}$. This practically means that we obtain a unique function $x_s(x_c)$ which covers not only the negative parity image, but also the second positive parity one, passing through the critical point (x_c^{cr}, x_s^{cr}) , which can be used to fix the position of the critical line in the cylindrical lens. This branch dies in x_c^{dis} where x_s reaches $x_s^{(3)}$. Finally, the principal image can be found solving Eq. (20) with the positive sign and the initial condition $x_s(x_c^{dis}) = x_s^{(1)}$. These choices correspond to the identification explained above between the images of the two frames. At the end, by Eq. (21), we get the final density profile for the cylindrical lens as a function of x_c .

In Fig. A1a we plot the relation between the positions of the images. Here we see that our choice has generated a relation which is necessarily discontinuous in $x_c = x_c^{dis}$. Then the outermost image is mapped in the sector $x_c > x_c^{dis}, x_s > x_s^{(1)}$, the negative parity image in $0 < x_c < x_c^{cr}, x_s^{cr} < x_s < x_s^{(2)}$ and the third image in the sector $x_c^{cr} < x_c < x_c^{dis}, x_s^{(3)} < x_s < x_s^{cr}$. As a consequence, also the cylindrical density profile is discontinuous. A simple way to smooth the discontinuity would be to allow the images of the cylindrical lens to carry a different weight in the total magnification than their corresponding spherical lens images.

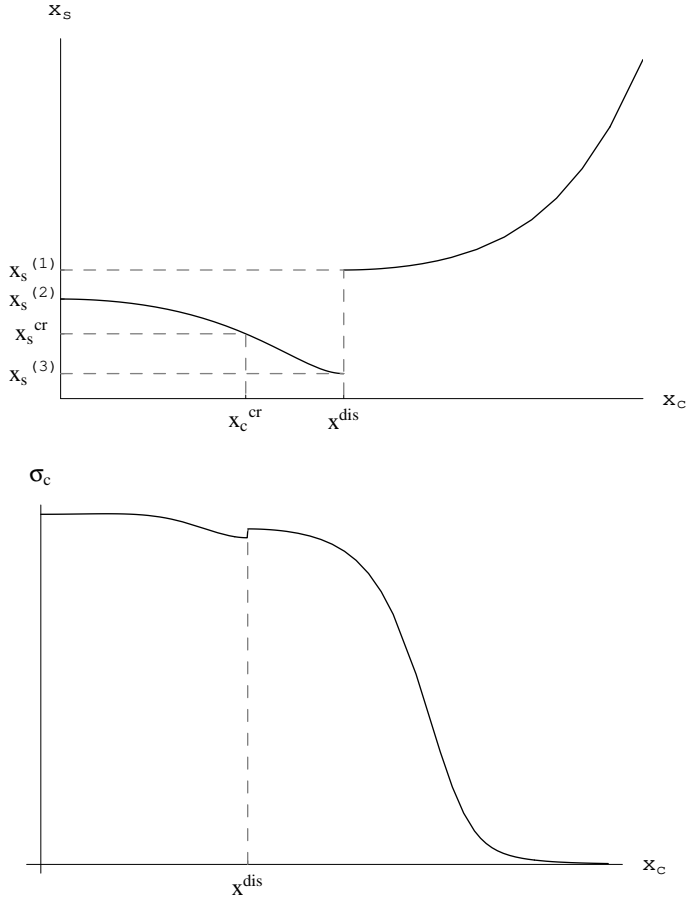


Figure A1. The same as figure 3 but starting from a higher spherical lens density and $b = 0.05$, in order to have caustic crossing and multiple image formation. (a) Relation between the spherical lens image positions x_s and the corresponding cylindrical lens image positions x_c . (b) The obtained cylindrical density profiles which reproduces the same caustic crossing microensing event as the original spherically symmetric lens.